Interparticle collision mechanism in turbulence

Jung-Il Choi,[1,*] Yongnam Park,[2] Ohjoon Kwon,[2] and Changhoon Lee[1,2,†]

[1]*Department of Computational Science and Engineering, Yonsei University, Seoul 120-749, South Korea*
[2]*Department of Mechanical Engineering, Yonsei University, Seoul 120-749, South Korea*

Direct numerical simulations of particle-laden homogeneous isotropic turbulence are performed to investigate interparticle collisions in a wide range of Stokes numbers. Dynamics of the particles are described by Stokes drag including particle-particle interactions via hard-sphere collisions, while fluid turbulence is solved using a pseudospectral method. Particular emphasis is placed on interparticle-collision-based conditional statistics of rotation and dissipation rates of the fluid experienced by heavy particles, which provide essential information on the collision process. We also investigate the collision statistics of collision time interval and angle. Based on a Lamb vortex model for a vortex structure, we claim that collision events occur in the edge region for vortical structures in the intermediate-Stokes-number regime, suggesting that the sling effect enhances collision as well as clustering.

I. INTRODUCTION

An understanding of interparticle collisions between small particles (or droplets) suspended in a turbulent fluid is necessary for describing important physical processes that are commonly found in natural phenomena and industrial problems such as rain formation and particle agglomeration [1]. Depending on the particle inertia, interactions between particles and background turbulence play an important role in collision process, which leads to nonlinearity of collision rates [2–5]. Extensive research [2–20] has focused on particle turbulence interactions in order to provide a reliable collision kernel, especially for particles of intermediate inertia considering preferential accumulation in regions of a low vorticity and high strain rate of background turbulence and the sling effect.

Turbulence-induced collision processes for the limiting cases of zero-inertia and high-inertia particles are already well understood [21,22]. The collision frequency for particles that are smaller than the Kolmogorov length scale is independent of particle properties [21], while the kinetic theory of gases was extended to incorporate the effect of high particle inertia on collision rates [22]. For particles of intermediate inertia, the influences of particle parameters such as response time, diameter, and number density on the collision frequency have been systematically investigated [2–5]. The relative velocity between two particles and the enhancement factor based on the radial distribution function measuring the effect of preferential concentration on the pair number density are used to describe geometrical collisions. It has been known that the turbulence-induced preferential concentration increases collision rates because of the accumulation of heavy particles towards low-vorticity and high-strain-rate regions and decorrelation of particle motion from the fluid. Recently, Voßkuhle *et al.* [19] proposed a collision mechanism based on clustering (mainly preferential concentration) and sling effects for inertia particles. The sling effect promotes interparticle collision due

to particles being slung by vortices when the particle response time is greater than the Komogorov time scale of flow. This phenomenon may be related to the fact that particles are trapped by or expelled from vortical structures depending on the relative ratio of time scales [23,24]. The rotational motion of such coherent vortical structures induces the centripetal force that is a dominant source of acceleration intermittency [25–27], which plays an important role in the sling effect. Previous studies have focused mostly on the modeling of a collision kernel based on the relative velocity between two particles and the radial distribution function or on the modeling of enhanced collisions based on the sling effect and caustics without providing a more detailed physical explanation for interactions between colliding particles and background turbulence. Therefore, it is necessary to understand the conditions under which interparticle collision mostly occurs and how the colliding particles interact with coherent vortical structures, which have not been investigated before.

The aim of this paper is to study how and where collision occurs by investigating collision-related statistics such as rotation and dissipation rates where collision takes place and interaction between particles and vortical structures using direct numerical simulation for a wide range of Stokes numbers (St). One unique nature of our study is the consideration of the binary collision process, which allows realistic simulation of particle motion even after collision. We consider interparticle collisions based on the hard-sphere collision model in isotropic turbulence at $Re_\lambda = 70$ by neglecting turbulence modulation due to particles and the gravity effect. Compared with two theoretical limits as well as other collision models, collision rates are characterized in terms of Stokes numbers. Statistics related to the number density, autocorrelations, and integral time scale of particles by performing the particle tracking with and without the collision model are obtained in order to examine the effect of interparticle collision on particle clustering. We investigate interactions between colliding particles and vortical structures using conditional statistics based on collision events for the rotation and dissipation rates of the fluid experienced by the particles. Relative motions between colliding particles are analyzed by collision angle and successive collision time interval. Moreover, a Lamb vortex

―――――――
*[*]jic@yonsei.ac.kr
[†]Corresponding author: clee@yonsei.ac.kr

model [28] is used to explain the interaction between vortical structures and particle motions. Finally, some insights into the collision process interacting with turbulence are illustrated in schematic collision diagrams.

II. NUMERICAL SIMULATIONS

Direct numerical simulations of isotropic turbulence at $Re_\lambda = 70$ with various Stokes numbers, ranging from 0.1 to 40, were performed to investigate the intercollision characteristics of heavy particles using a pseudospectral method. Note that Re_λ denotes the Taylor-scale Reynolds number, and the Stokes number is defined as the ratio of the particle response time ($\tau_p = \rho_p d_p^2/18\mu$) to the Kolmogorov time scale (τ_η) of turbulence: $St = \tau_p/\tau_\eta$. Here, d_p and μ are the diameter of the particle and the viscosity of the fluid, respectively. To maintain stationary statistics in turbulence, we used the forcing scheme utilizing Uhlenbeck-Ornstein random processes [29]. For forcing parameters, the maximum forcing wavenumber K_f is set to $2\sqrt{2}$ and the time scale T_L^f and standard deviation σ_f^2 in the Langevin equation are chosen as 0.4312 and 0.1276, respectively. The fluid domain (a cube of size 2π) is uniformly discretized with 128^3 grid points. Details of the numerical methods are given by Jung *et al.* [24] and Abdelsamie and Lee [30].

Under the assumption for heavy particles, all the transient drags are negligible in the BBO (Basset-Boussinesq-Oseen) equation of motion [31]. Thus, simplified equations of particle motion including particle-particle collisions can be written as

$$\frac{d\mathbf{v}_p}{dt} = \frac{1}{\tau_p}(\mathbf{u} - \mathbf{v}_p) + \mathbf{a}_c \quad \text{and} \quad \frac{d\boldsymbol{\omega}_p}{dt} = \frac{10}{3\tau_p}(\boldsymbol{\omega} - \boldsymbol{\omega}_p), \quad (1)$$

where $\mathbf{u}$ and $\boldsymbol{\omega}$ are the instantaneous fluid velocity and angular velocity, which is half of the vorticity, at the particle position, while $\mathbf{v}_p$ and $\boldsymbol{\omega}_p$ are the instantaneous particle velocity and particle angular velocity, respectively. It should be noted that information on the particle angular velocity is necessary for collision modeling. To obtain flow quantities at the locations of the particles, the four-point Hermite interpolation scheme was used, while particles were tracked using the third-order Runge-Kutta time advancement scheme [32–34]. The hard-sphere collision model [35] was used to determine the acceleration ($\mathbf{a}_c$) caused by collision forces based on the conservation law of momentum and angular momentum for collisions without energy loss (perfect elastic collisions). We also used the same detection procedure for interparticle collisions as in Ref. [36], which is based on a geometric solution of relative displacements of any pairs of colliding particles. For the interparticle collision, we updated the particle velocities in the precollision state by the postcollision velocities. Randomly distributed monodisperse particles with $d_p/\eta = 0.34$ are considered in the present study. The total number of released particles is $N_p = 2 \times 64^3$ for all Stokes numbers and the volume fraction of the particles is less than 0.1%. Therefore, due to the dilute dispersion of particles, the turbulence modulation by particles is neglected. The computation time required for our study of particle collision statistics is much more demanding compared to pure turbulence simulations for three reasons. First, we used a costly but very accurate interpolation scheme such as the fourth-order Hermite scheme in our Lagrangian particle

TABLE I. Flow properties and numerical simulation conditions. The reference length scale is the computational domain length 2π and the reference time scale is $(\pi/\epsilon)^{1/3} \sim 1$.

N	Re_λ	$\kappa_m\eta$	u'	ϵ	L	λ	τ_η
128^3	70	1.5	2.58	9.18	0.984	0.405	0.040

tracking algorithm [32]. Second, although we used an efficient algorithm for detecting collision between two particles by checking only nearby particles, this process requires a great deal of computation time, as the number of particles increases. Finally, but most intensively, in order to obtain fully converged statistics conditional on collision, a much longer integration time is necessary than when pure Lagrangian statistics are computed without considering collision since collision does not occur as frequently. For this reason, we did not consider cases with Reynolds numbers higher than the current one.

Fundamental flow properties for the forced isotropic turbulence are summarized in Table I. The Kolmogorov microscale is

$$\eta = (\nu/\epsilon)^{1/4}, \quad (2)$$

and the Taylor microscale is

$$\lambda = (15\nu/\epsilon)^{1/2}u', \quad (3)$$

where ϵ is the energy dissipation rate, ν is the kinematic viscosity of the fluid, and u' is the root-mean-squared velocity. The integral length scale is defined as

$$L = \frac{\pi}{2u'^2} \int_0^{k_{\max}} k^{-1} E(k)\, dk, \quad (4)$$

where $E(k)$ is the energy spectrum and $k_{\max}$ is the largest wave number, satisfying $k_{\max}\eta = 1.5$. Although this resolution is marginal for resolving the intermittent nature of rotation or dissipation, it is enough for extracting the prominent characteristics of collision-conditioned statistics which are shown later.

III. RESULTS AND DISCUSSION

A. Collision rate

The dependency of the steady-state collision frequency on the Stokes numbers is shown in Fig. 1. We have also plotted two theoretical limits: Saffman and Turner theory for noninertial particles [21] and kinetic theory for large/dense particles [22] as well as other collision frequency models described by Wang *et al.* [4] and Zaichik *et al.* [5]. Similarly to findings of Sundaram and Collins [2], the collision frequencies for finite-inertia particles from the present simulations are higher than that for the Saffman-Turner limit and lower than that for kinetic theory but asymptotically approach both theoretical limits. We also found that the maximum of the collision frequency is at about $St = 4$. This can be explained by two competing phenomena: (i) preferential concentrations in high-strain and low-vorticity regions and (ii) crossing trajectory effects (see Fig. 5 of Jung *et al.* [24]). Therefore, an intermediate-Stokes-number [$St \approx O(1)$] regime shows a high collision frequency when particles are accumulated
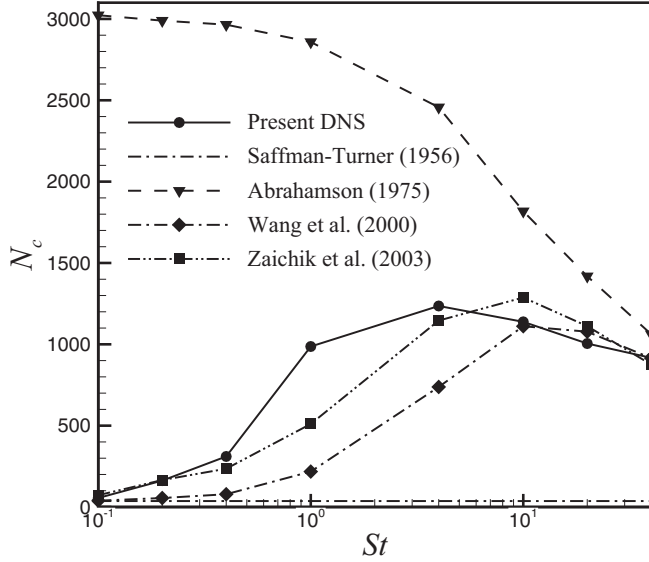
FIG. 1. Interparticle collision rates for different Stokes numbers at $Re_\lambda = 70$.

near vortical structures due to interaction between suspended particles and background turbulence, but at the same time the particles are decorrelated with the background turbulence enough to cross the vortical structures. Our predictions show some differences from the results of Wang *et al.* [4] in the low- and intermediate-Stokes-number range and of Zaichik *et al.* [5] at intermediate Stokes numbers. The model of Zaichik *et al.* [5] is based on statistical modeling which did not consider the effect of coherent structures and clustering of particles, possibly underpredicting the collision frequency for particles of Stokes number of order 1. The model of Wang *et al.* [4] did not consider the physical collision process, thus allowing overlapping of the particle volume in the collision event. This cannot capture the effect of finite-size particles after collision, which is expected to add randomness to the particle behavior, thus possibly underestimating the collision frequency for small-Stokes-number particles as well as for intermediate Stokes numbers.

B. Particle clustering

Collision rates are known to be closely related to the particle preferential concentration depending on the Stokes number [2]. To clarify whether interparticle collision enhances or mitigates the preferential concentration, we investigate the statistics for particle behaviors by performing particle tracking with and without the collision model. The probability density functions (PDFs) of the number density are plotted in Fig. 2(a) for different Stokes numbers in order to investigate the effect of collision on the preferential concentrations. Note that the number density (n_p) is defined as the ratio of the number of particles in a small box to its volume. Since we used 64^3 boxes to estimate the density, the box size is about 0.098^3, which is equivalent to $(4.3\eta)^3$. Although the number density itself depends sensitively on the choice of box size as pointed out by Monchaux *et al.* [37], our objective here is to investigate the relative effect of collision on particle clustering. There is no
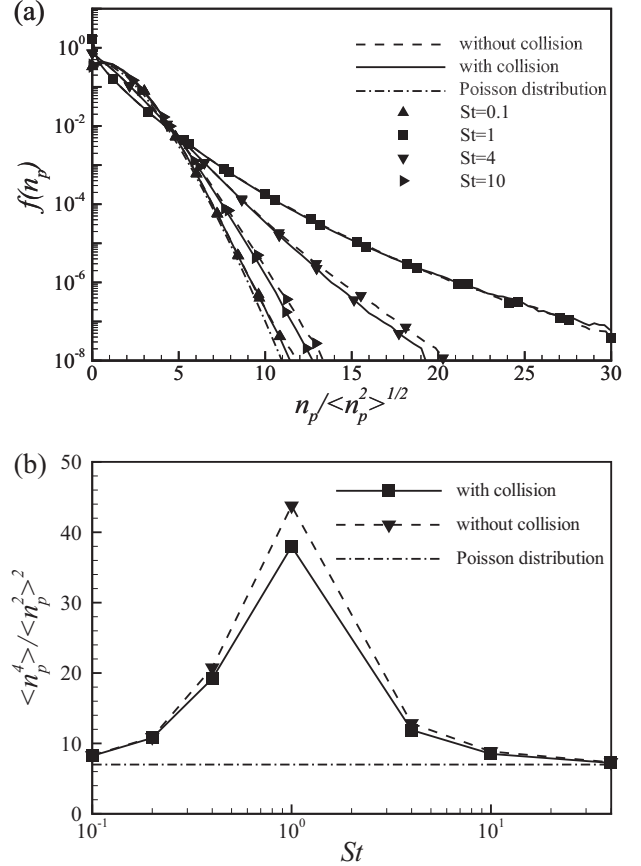

FIG. 2. Effect of interparticle collision on particle clustering: (a) probability density function (PDF) and (b) flatness of the particle number density. Solid and dashed lines represent the PDFs of number density with and without the collision model, respectively.

obvious difference in the PDFs of the number density between cases with and cases without interparticle collision. In both cases, a long tail of the PDF is observed when St $= 1$, while the PDFs for St $= 0.1$ and 40 are similar to the PDF of a fluid particle. Such a long tail of the PDF at St $= 1$ reflects localized high concentrations of the particles.

It is also shown in Fig. 2(b) that the flatness of the number density ($\langle n_p^4 \rangle / \langle n_p^2 \rangle^2$) in both cases is maximized at St $= 1$, while the flatness for St $\ll 1$ or St $\gg 1$ asymptotically converges to 7. Due to the collision, the particle clustering is slightly suppressed, which leads to a decrease in the maximum flatness near St $= 1.0$. Note that the PDF of randomly distributed particles following a Poisson distribution is defined as $p(n) = \mu_m^n e^{-\mu_m} / n!$, where n is the number of particles in a cell and μ_m is the mean value. The flatness of the Poisson distribution is $\mu_m^{-1} + 3$. Since the mean number in the present study is $\mu_m = 2 \times 64^3 / 128^3 = 1/4$, the asymptotic value for the present direct numerical simulation results is in good agreement with that for the Poisson distribution. Consequently, a high collision rate is expected at the intermediate Stokes numbers [St $\approx O(1)$] due to the preferential concentrations. However, it is noteworthy that the maximum collision rate and maximum flatness of the number density occur at different Stokes numbers. This implies that an interplay between particles and background turbulence influences the increase
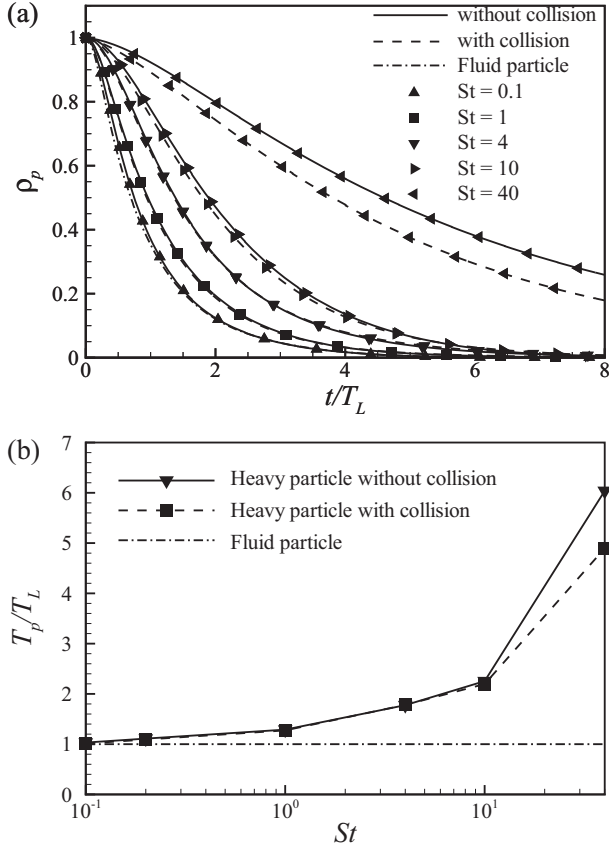
FIG. 3. Effect of interparticle collision on (a) the autocorrelation function and (b) the integral time scale of the particle velocity. Solid and dashed lines represent the autocorrelations with and without the collision model, respectively.
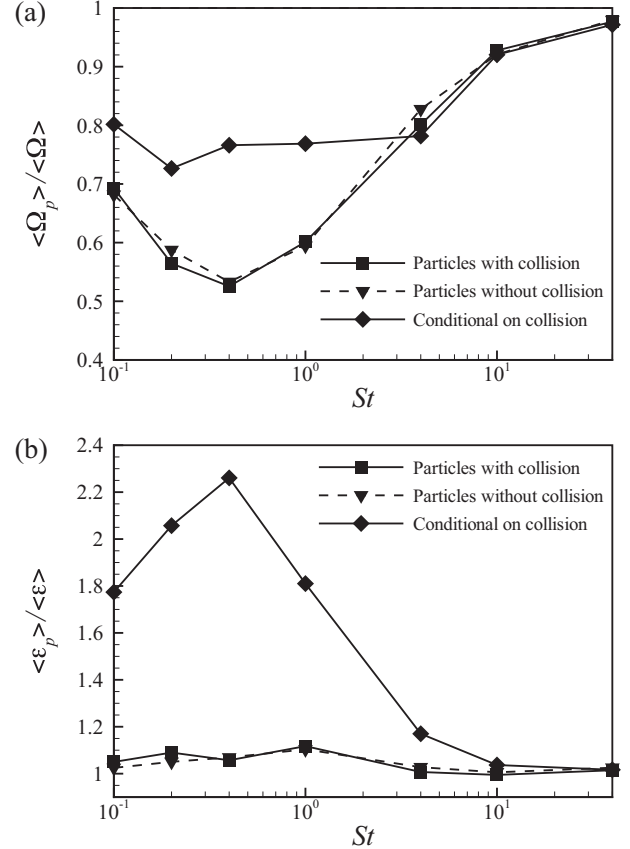

FIG. 4. Effect of interparticle collision on (a) the fluid rotation rate and (b) the dissipation rate at particle locations with the corresponding statistics conditional on collision.

in the collision rate at St > 1. For maximum collision events, both the preferential concentration and the finite-inertia effect are equally necessary.

For statistically stationary turbulence, the Lagrangian auto-correlation function $\rho_p(t)$ is defined as

$$\rho_p(t) = \frac{\langle v_p(t_0)v_p(t + t_0)\rangle}{\langle v_p^2(t_0)\rangle}, \quad (5)$$

where t_0 is the reference time and its integral time scale is

$$T_p = \int_0^\infty \rho_p(t)dt. \quad (6)$$

Figure 3 shows the effect of interparticle collision on the ρ_p of the particle velocity and normalized integral time scale T_p/T_L, with T_L denoting the Lagrangian integral time scale of fluid particles. General trends show that ρ_p extends further as the Stokes number increases due to the fact that a heavier particle has more inertia [24]. When collision is considered, ρ_p shows an apparently quicker decay for St > 10 than in the case without collision. Accordingly, T_p is reduced due to the collision for higher-Stokes-number particles. This indicates that temporal memory effects of particle motion are weakened and decorrelated after interparticle collisions. Given that the dispersion coefficient is proportional to the mean-squared particle velocity and the integral time scale

[24,38,39], the decrease in the integral time scale for high Stokes numbers indicates less dispersion since the kinetic energy of particles is conserved through elastic collision process. Adding randomness through collision interestingly suppresses dispersion.

To determine the cause of the high collision frequency at intermediate Stokes numbers, we investigated the statistics of rotation (=enstrophy) and dissipation rates of fluid seen by particles with and without interparticle collisions. We also plot the averaged enstrophy and dissipation rates of fluid seen by only colliding particles in Figs. 4(a) and 4(b), respectively. The statistics are normalized by their values for the noninertial particles (fluid particles). There are no obvious differences in the statistics for the simulation results with versus without the collision model. Particles with finite inertia still tend to accumulate in a preferential region of low rotation rate before or after the interparticle collision. However, the conditional statistics indicate that colliding particles below the intermediate-Stokes-number regime (St < 4) have a higher vorticity and higher dissipation rate than noncolliding particles. This is an important observation, that particles with St ~ $O(1)$ collide with each other preferably where fluid rotation and dissipation are stronger than the averaged values over all particle positions. This implies that particles with St ~ $O(1)$ having highly intermittent accelerations in a core of vortical structure escape from the vortical structures due

to centrifugal forces and then collide with particles still near the vortical structures. Even particles with a very small Stokes number, St ∼ 0.1, show similar behavior, which is surprising since particles with a small Stokes number almost follow fluid particles and fluid particles tend to disperse homogeneously. This can be understood by the observation that the Lagrangian statistics of rotation and dissipation show quite an intermittent nature [40].

C. Collision statistics

In this section, we investigate collision statistics such as the collision angle (θ_C) and collision time interval (t_C) to understand how collision occurs. For a pair of colliding particles, a collision angle (θ_C) is defined as the angle between the velocity vectors of the particles just before collision. The PDF of the collision angle shown in Fig. 5(a) indicates that the most probable collision angle is 0 for small Stokes numbers (St ≪ 1), while the PDF becomes flat and symmetric as the Stokes number increases. Note that the PDF of the angle (θ) between two random vectors is $p(\theta) = (\sin \theta)/2$ [41]. This implies that two particles stream together rather than colliding with each other for small Stokes numbers, but the probability of head-on collision increases as the Stokes number increases. Since the particle motion for large Stokes numbers (St ≫ 1) is mainly governed by the particle inertia, collisions with an arbitrary angle are expected due to the decorrelated particle motions from the background turbulence. It should be noted that the maximum probability is observed at $\theta_C = 5°$ when St = 4, while the angle where the maximum probability is found when St ⩽ 1 is 0. This clearly indicates that most active collisions require inertia to a certain extent.

The behavior of the collision angle for different Stokes numbers can be understood by the formation of caustics. As St → 0, the particle velocity is the single-valued function of the position and, thus, can be considered to be continuously distributed in space. The only way to have a collision between two particles is through tangential contact by the shearing motion [21]. As the Stokes number increases, however, the single-valuedness of the particle velocity breaks down due to the nonlinearity which is present in the governing equation of the velocity gradient of the particles [8,11]. Then the particle velocity is multivalued and particles at the same position move at different velocities, which is a typical symptom when caustics form [10], resulting in a collision with a finite collision angle.

The collision time interval (t_C) is defined as the interval between two successive collisions of each particle. Figure 5(b) shows the PDF of the collision intervals. When the collision interval time is smaller than the Kolmogorov time scale ($t_C ⩽ \tau_\eta$), corresponding events are excluded from the statistics computation in order to avoid the false collision detection of two streaming particles due to numerical errors. For small Stokes numbers, most interparticle collisions are observed within a short time interval ($t_C/\tau_\eta < 20$), but the collision event is rare, which means that particles aligned with each other tend to collide successively, but most particles stream without collision. However, the PDF shows an exponential decay at long collision time intervals for intermediate and large Stokes numbers (St ⩾ 1), which is typically observed
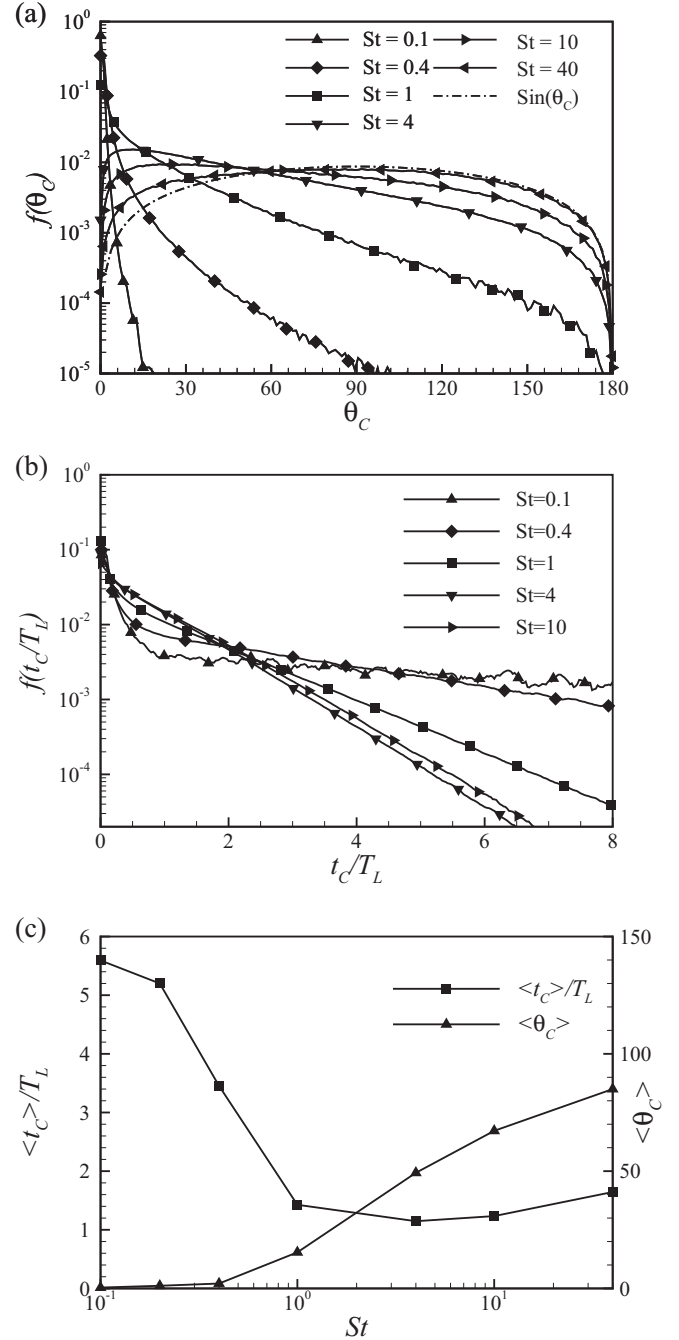

FIG. 5. Probability density functions of (a) the collision angle (deg) and (b) the normalized collision time interval, and (c) the averaged collision angle (deg) and normalized time interval for different Stokes numbers.

in the distribution of the time interval between two random collisions by Cate *et al.* [42].

The ensemble mean of the collision angle $\langle \theta_C \rangle$ in Fig. 5(c) clearly summarizes our observation that most interparticle collision events in the small-Stokes-number regime occur when two particles are streaming around the vortical structures. For the large-Stokes-number regime, the probability of a random head-on collision is increased and the averaged collision angle approaches $\pi/2$. Also, the averaged collision interval time
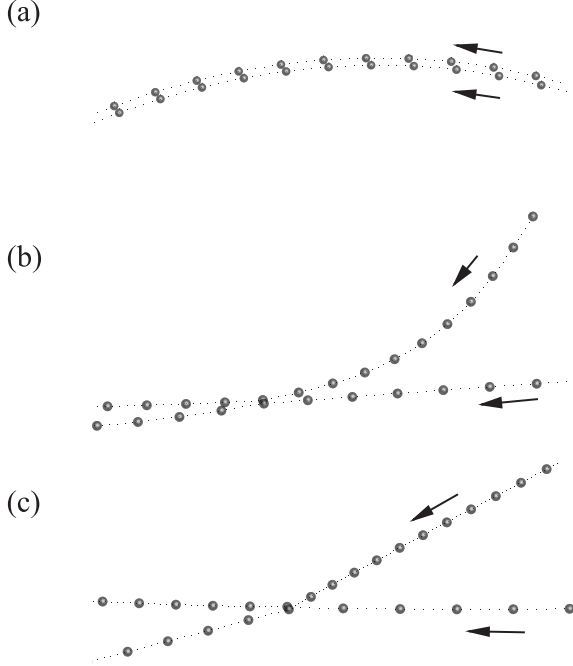
(a)

(b)

(c)

FIG. 6. Trajectories of two particles before and after a collision event for (a) St = 0.1, (b) St = 1, and (c) St = 10.

$\langle t_C \rangle$ is larger in the small-Stokes-number regime, while the local minimum of the collision interval is observed at St = 4, which corresponds to the local maximum of collision rates in the intermediate-Stokes-number regime. The dependency of the ensemble means on the Stokes number is consistent with the results of Ernst and Sommerfeld [17].

Figure 6 shows snapshots of the computed trajectories of two particles before and after a collision event for different Stokes numbers. For St = 0.1, collision is clearly due to shearing motion and two particles are streaming on a curved path even after the collision, which indicates that there is no significant momentum exchange and its collision angle is almost 0°. For St = 1, two particles are streaming with a smaller postcollision angle compared to the precollision angle after a particle following a curved path line collides with another particle in a straight motion that probably is slung out of a vortex core. This implies that the collision event occurs near the boundary of the vortical structure. For St = 10, two particles in rectilinear motions collide with each other, which indicates a random collision event.

D. Collision picture

Based on our observation that collision-conditioned rotation and dissipation rates are clearly more pronounced as shown in Fig. 4, we investigate in this section the rotation/dissipation structure of an isolated vortex representing turbulent structures. This provides a better idea of the role of vortical structures in particle collisions. Vortices in turbulence have been known as the source of adjacently found intermittently large rotation and dissipation rates [26,43]. In order to take advantage of this, we consider a simple vortex model which possesses such a property. Recently, Lee *et al.* [28]
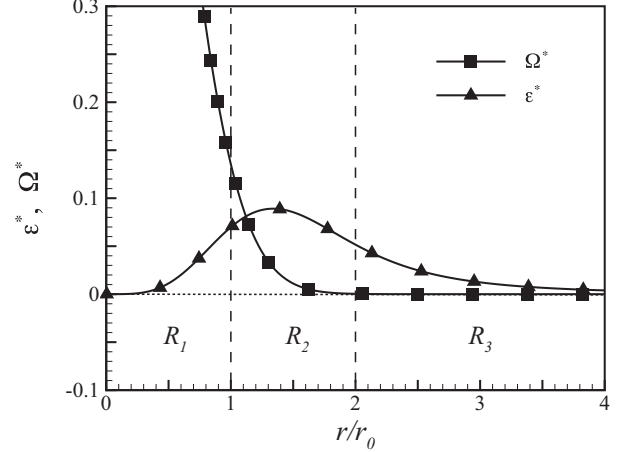

FIG. 7. Radial distributions of normalized enstrophy and normalized dissipation for the Lamb vortex model.

used the Lamb vortex model to explain the strong acceleration intermittency in turbulence in terms of the local enstrophy and dissipation, both of which are relevant to the rotational motion of vortex filaments. The Lamb vortex is a cylindrical vortex defined by the circumferential velocity v_θ, given by

$$v_\theta = \frac{\Gamma}{2\pi r}\left[1 - \exp\left(-\frac{r^2}{r_0^2}\right)\right], \tag{7}$$

where Γ and r_0 are the circulation strength and the core radius, respectively. The corresponding normalized enstrophy (Ω^*) and dissipation (ε^*) can be obtained,

$$\Omega^* = \frac{\Omega}{\Gamma^2/2\pi^2 r_0^4} = \left[\exp\left(-\frac{r^2}{r_0^2}\right)\right]^2, \tag{8}$$

$$\varepsilon^* = \frac{\varepsilon/2\nu}{\Gamma^2/2\pi^2 r_0^4} = \left[\left(\frac{r_0^2}{r^2} + 1\right)\exp\left(-\frac{r^2}{r_0^2}\right) - \frac{r_0^2}{r^2}\right]^2. \tag{9}$$

Figure 7 shows the radial distributions of Ω^* and ϵ^* for the Lamb vortex in a bounded domain $0 < r < R$ with $R/r_0 = 4$. Note that $\epsilon^*(R)$ is less than 5% of the peak value of ϵ^*. This kind of adjacent peak of rotation and dissipation rate was typically observed near a vortical structure in turbulence [26]. The local enstrophy decreases monotonically as r increases, while the local peak of dissipation is found at $r = 1.34r_0$, where intermittently high acceleration is found [28]. Although the Lamb vortex cannot describe the nature of most vortices in turbulence, it possesses some intermittent characteristics of dissipation and enstrophy found in turbulence. For example, the distributions of powered dissipation of the Lamb vortex and vortices in turbulence are similar. The distribution of dissipation of the Lamb vortex [Eq. (9)] can be approximated by $\varepsilon \sim r^{-4}$ except for the core of the vortex, which leads to a power-law distribution of the PDF of n-powered dissipation, $f(\varepsilon^n) \sim (\varepsilon^n)^{-(2n+1)/2n}$. As n goes higher, the PDF approaches $\sim(\varepsilon^n)^{-1}$. This behavior can be found in the PDF of ε^n for higher n's in the large-magnitude tail part obtained from isotropic turbulence as shown in Fig. 8(a), although the PDF for low n's does not show such a power-law distribution as suggested by the Lamb vortex model. This implies that
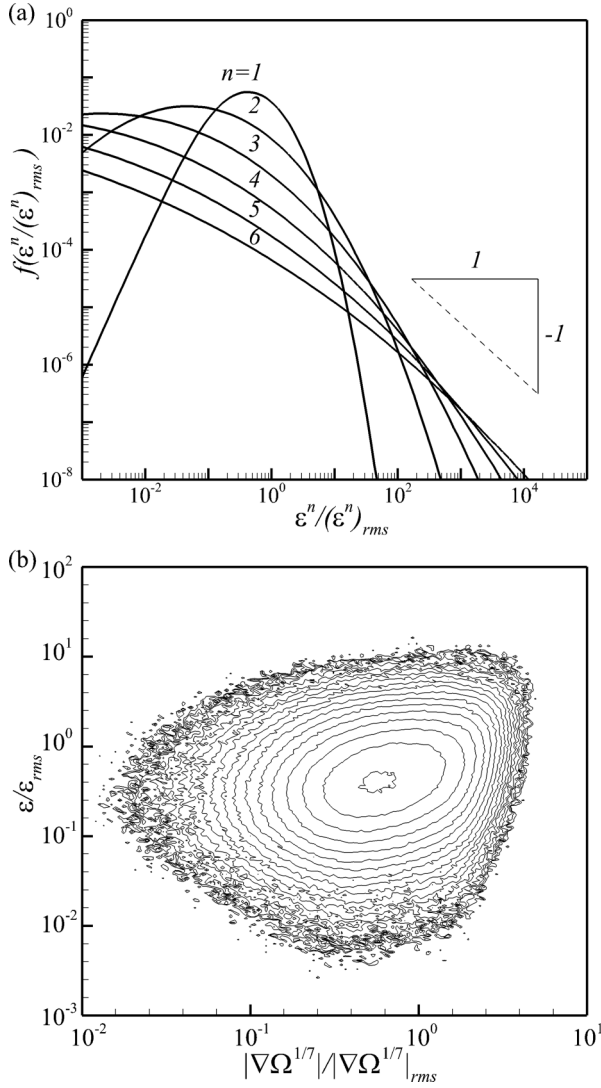
TABLE II. Region-averaged normalized enstrophy and dissipation for the Lamb vortex.

Region	R_1	R_2	R_3	$R_2 \cup R_3$	$R_1 \cup R_2 \cup R_3$
$\langle \Omega^* \rangle$	0.597	0.028	0.000	0.009	0.156
$\langle \epsilon^* \rangle$	0.021	0.077	0.017	0.037	0.033

in Table II. Except for the core region (R_1), the region-averaged enstrophy is lower than the average value (0.156) over the whole domain. This is due to the extremely high enstrophy in the core region. On the other hand, the dissipation in the edge region (R_2) is 2.3 times higher than the total average. Analogous to the Lamb vortex, the present direct numerical simulation results for rotation rate and dissipation conditional on collision in Fig. 4 indicate that particles colliding in the case of St < 4 are rarely observed in a core region of vortical structures where the rotation rate is high. More importantly, conditional statistics of dissipation suggest that the collision mainly occurs at the edge of a vortex such as the R_2 region of the Lamb vortex. Although the Lamb vortex model is a simple model and thus cannot completely represent a vortical structure in turbulence, the intermittently large dissipation found at the edge of a vortex clearly captures the real nature of turbulence. Therefore, our observation of enhanced collision-conditioned dissipation safely leads to our conjecture that collisions occur at the edge of vortices when St $\sim$ 1.

Based on our observation of particle trajectories, collision angle statistics, and analogy to a simple vortex model, we propose plausible pictures of interparticle collision for three Stokes number regimes. For small Stokes numbers (St $\ll$ 1), interparticle collisions seem to occur in a shearing motion when suspended particles near vortical structures follow converging streamlines around the vortices. Moreover, a particle tends to collide repeatedly with other particles moving in the same direction. For intermediate Stokes numbers [St $\approx O(1)$], due to the preferential concentrations, particles are accumulated near vortical structures. Collisions seem to occur when particles having relatively high acceleration near vortical structures are moving away from the structures due to centrifugal forces. Collision rates are enhanced by the preferential concentrations towards strong vortical and straining flow structures and a moderate (or efficient) decorrelation of the particle motion from the fluid. For large Stokes numbers (St $\gg$ 1), particle motions become completely decorrelated from the fluid structures and the collision process tends to be random. Collision rates are decreased with longer particle response times, approaching the values predicted by the kinetic theory.

IV. CONCLUSIONS

Characteristics of interparticle collision in isotropic turbulence at Re$_\lambda$ = 70 were investigated using direct numerical simulation with explicit treatment of collision process. The maximum collision frequency was observed at an intermediate Stokes number (St = 4), while the collision rate varied with the Stokes number. We found that the number density distribution of the particles and statistics of the fluid seen by particles

FIG. 8. (a) PDF of ε^n and (b) contours of the joint PDF between ε and $|\nabla \Omega^{1/7}|$ obtained from direct simulation of isotropic turbulence.

intermittently large dissipation in turbulence shares similar statistical properties with the Lamb vortex. Further observation of the distributions of enstrophy and dissipation given by Eqs. (8) and (9) yields that there exists an exponent α such that $d\Omega^\alpha/dr$ has a local maximum at the same radial distance, $r = 1.34r_0$, as dissipation. α turns out to be $\sim 1/7$. This suggests that $|\nabla \Omega^{1/7}|$ and local dissipation in real turbulence can be highly correlated in the high-amplitude region if the Lamb vortex captures the structural characteristics of vortices in turbulence very well. The joint PDF obtained from isotropic turbulence indeed shows some correlation between these two quantities in the high-amplitude region as shown in Fig. 8(b), whereas $|\nabla \Omega|$ and dissipation do not show such a correlation. This provides the rationale behind our use of the Lamb vortex in the interpretation of the behavior of collision-conditioned enstrophy/dissipation.

The three regions $R_1 = [0, r_0]$, $R_2 = [r_0, 2r_0]$, and $R_3 = [2r_0, R]$ in Fig. 7 represent the core, edge (or transition), and outer regions of a vortex, respectively. The region-averaged enstrophy and dissipation for the Lamb vortex are summarized

are not significantly influenced by the interparticle collisions, except for the autocorrelation of the particle velocity for large Stokes numbers. Conditional statistics for the rotation and dissipation rates of the fluid seen by colliding particles provided evidence of the collision mechanism in the intermediate-Stokes-number regime, where particles with highly intermittent accelerations near the core of vortical structures collided with other particles at the edge of the vortical structures. The collision angle and time interval showed that most of the collision process for small Stokes numbers is a contact between a pair of aligned particles, while for large Stokes numbers, the collision is random with a nonpreferential collision angle due to the decorrelated particle motion from the background turbulence. For intermediate Stokes numbers, particles tend to collide at a small but finite angle, displaying the effect of caustics. Utilizing the Lamb vortex model, we conjecture that most collision events occur in the edge region for vortical structures in the intermediate-Stokes-number regime. After all, the sling effect directly enhances collision as well as causing preferential concentration, which also increases the collision rate.

Although our investigation was carried out for a very limited range of parameters such as Reynolds number and particle size, the overall qualitative picture of collision would not be so different from what we found in this study since the basic mechanism of particle collision is associated with the vortical structures of turbulence, which are typically of a small scale such as the Kolmogorov length scale. Due to the intensive nature of the computing time for collision detection, we could not investigate the behavior of particles at high Reynolds numbers. Instead, as a preliminary study we had tested a lower-Reynolds-number case with a 64^3 resolution. Qualitatively similar behavior of particles was observed. For example, the mean dissipation conditional on a collision event with St ~ 1 clearly shows an enhanced value, with almost the same peak value as in Fig. 4(b). Although how the statistics change with higher Reynolds number is not clear, we carefully predict that quantitative change of statistics with Reynolds number would not modify our picture of collision found in the current study. The better knowledge of the collision mechanism obtained in our study will benefit collision modeling in rain formation or other engineering applications such as spray. We have not considered the effect of gravity, which is essential in real collision processes in clouds, suggesting a future extension of the current study. Our other works on gravity [33,44] indicate that gravity causes vertical clustering and the settling motion of particles suppresses the sling effect, which definitely affects collision.

[1] W. Grabowski and L.-P. Wang, Annu. Rev. Fluid Mech. **45**, 293 (2013).

[2] S. Sundaram and L. R. Collins, J. Fluid Mech. **335**, 75 (1997).

[3] W. C. Reade and L. R. Collins, Phys. Fluids **12**, 2530 (2000).

[4] L.-P. Wang, A. S. Wexler, and Y. Zhou, J. Fluid Mech. **415**, 117 (2000).

[5] L. I. Zaichik, O. Simonin, and V. M. Alipchenkov, Phys. Fluids **15**, 2995 (2003).

[6] J. Eaton and J. Fessler, Int. J. Multiphase Flow **20**, 169 (1994).

[7] A. Aliseda, A. Cartellier, F. Hainaux, and J. Lasheras, J. Fluid Mech. **468**, 77 (2002).

[8] G. Falkovich, A. Fouxon, and M. G. Stepanov, Nature **419**, 151 (2002).

[9] L.-P. Wang, C. N. Franklin, O. Ayala, and W. W. Grabowski, J. Atmos. Sci. **63**, 881 (2006).

[10] M. Wilkinson, B. Mehlig, and V. Bezuglyy, Phys. Rev. Lett. **97**, 048501 (2006).

[11] G. Falkovich and A. Pumir, J. Atmos. Sci. **64**, 4497 (2007).

[12] O. Ayala, B. Rosa, and L.-P. Wang, New J. Phys. **10**, 075016 (2008).

[13] J. Salazar, J. de Jong, L. Cao, S. Woodward, H. Meng, and L. Collins, J. Fluid Mech. **600**, 245 (2008).

[14] E. Saw, R. Shaw, S. Ayyalasomayajula, P. Chuang, and A. Gylfason, Phys. Rev. Lett. **100**, 214501 (2008).

[15] L.-P. Wang, B. Rosa, H. Gao, G.-W. He, and G. Jin, Int. J. Multiphase Flow **35**, 854 (2009).

[16] R. Monchaux, M. Bourgoin, and A. Cartellier, Phys. Fluids **22**, 10304 (2010).

[17] M. Ernst and M. Sommerfeld, J. Fluid Eng. **134**, 031302 (2012).

[18] R. Onishi and J. C. Vassilicos, J. Fluid Mech. **745**, 279 (2014).

[19] M. Voßkuhle, A. Pumir, E. Lévêque, and M. Wilkinson, J. Fluid Mech. **749**, 841 (2014).

[20] M. Obligado, T. Teitelbaum, A. Cartellier, P. Mininni, and M. Bourgoin, J. Turbul. **15**, 293 (2014).

[21] P. G. Saffman and J. S. Turner, J. Fluid Mech. **1**, 16 (1956).

[22] J. Abrahamson, Chem. Eng. Sci. **30**, 1371 (1975).

[23] L. Biferale, G. Boffetta, A. Celani, A. Lanotte, and F. Toschi, Phys. Fluids **17**, 021701 (2005).

[24] J. Jung, K. Yeo, and C. Lee, Phys. Rev. E **77**, 016307 (2008).

[25] C. Lee, K. Yeo, and J.-I. Choi, Phys. Rev. Lett. **92**, 144502 (2004).

[26] S. Lee and C. Lee, Phys. Rev. E **71**, 056310 (2005).

[27] Y. Choi, Y. Park, and C. Lee, Int. J. Heat Fluid Flow **31**, 482 (2010).

[28] C. Lee, Y. Park, and J. Jung, J. Mech. Sci. Tech. **26**, 3843 (2012).

[29] V. Eswaran and S. B. Pope, Comput. Fluids **16**, 257 (1988).

[30] A. H. Abdelsamie and C. Lee, Phys. Fluids **24**, 015106 (2012).

[31] M. R. Maxey and J. J. Riley, Phys. Fluids **26**, 883 (1983).

[32] J.-I. Choi, K. Yeo, and C. Lee, Phys. Fluids **16**, 779 (2004).

[33] Y. Park and C. Lee, Phys. Rev. E **89**, 061004(R) (2014).

[34] J. Lee and C. Lee, Phys. Fluids **27**, 023303 (2015).

[35] C. Crowe, J. Schwarzkopf, M. Sommerfeld, and Y. Tsuji, *Multiphase Flows with Droplets and Particles*, 2nd ed. (CRC Press, Boca Raton, FL, 2012).

[36] N. Gui, J. R. Fan, and K. Cen, Phys. Rev. E **78**, 046307 (2008).

[37] R. Monchaux, M. Bourgoin, and A. Cartellier, Int. J. Multiphase Flow **40**, 1 (2012).

[38] G. K. Batchelor, Aust. J. Sci. Res. Ser. A **2**, 437 (1949).

[39] A. H. Abdelsamie and C. Lee, Phys. Fluids **25**, 033303 (2013).

[40] P. K. Yeung, S. B. Pope, E. A. Kurth, and A. G. Lamorgese, J. Fluid Mech. **582**, 399 (2007).

[41] J. van Pelt and H. B. M. Uylings, Front. Comput. Neurosci. **5**, 54 (2012).

[42] A. T. Cate, J. J. Derksen, L. M. Portela, and H. E. A. V. D. Akker, J. Fluid Mech. **519**, 233 (2004).

[43] B. W. Zeff, D. D. Lanterman, R. McAllister, R. Roy, E. J. Kostelich, and D. P. Lathrop, Nature **421**, 146 (2003).

[44] I. Fouxon, Y. Park, R. Harduf, and C. Lee, Phys. Rev. E **92**, 033001 (2015).